3D Printed Bioplastics with Shape-Memory Behavior Based on Native Bovine Serum Albumin

Eva Sanchez-Rexach,[†,‡] Patrick T. Smith,[‡] Alvaro Gomez-Lopez,[†] Maxence Fernandez,[§] Aitziber L. Cortajarena,[§,‖] Haritz Sardon[*,†], and Alshakim Nelson*[*,‡]*

[†]POLYMAT, University of the Basque Country UPV/EHU, Donostia-San Sebastian, Spain

[‡]Department of Chemistry, University of Washington, Seattle, WA, USA

[§]Center for Cooperative Research in Biomaterials (CIC biomaGUNE), Basque Research and Technology Alliance, Donostia-San Sebastian, Spain

[‖]Ikerbasque, Basque Foundation for Science, 48009 Bilbao, Spain

ABSTRACT: Bio-based plastics that can supplant petroleum-derived materials are necessary to meet the future demands of sustainability in the life cycle of plastic materials. While there are significant efforts to develop protein-based plastic materials for commercial use, their application is limited by poor processability and limitations in mechanical performance. Here, we present a bovine serum albumin (BSA)-based resin for stereolithographic apparatus (SLA) 3D printing that affords bioplastic objects with shape memory behavior. We demonstrate that the native conformation of these globular proteins is largely retained in the 3D printed constructs, and that each protein molecule possesses a "stored length" that could be revealed during mechanical deformation (extension or compression) of the 3D bioplastic objects. While the plastically

deformed objects could retain this state for an indefinite period of time, heating the object or submerging in water allowed it to return to its original 3D printed shape.

1. INTRODUCTION

Bio-sourced materials that can supplant petroleum-based materials are an integral component of sustainability. Moreover, renewable materials with greater complexity and functionality will be required to meet the demands for the full spectrum of applications from aerospace to medicine. Protein-based materials, which include biologically derived proteins, engineered proteins, and polymer-protein conjugates, have been developed to create materials that emulate biological and nonbiological function, as well as other physical characteristics (i.e., mechanical properties).[1-5] While there are significant efforts to develop protein-based plastic materials for commercial use, their application is restricted by poor processability into 3D form factors and limitations in mechanical performance.[6] Both 3D and 4D additive manufacturing (AM) processes that utilize vat photopolymerization have tremendous potential in industrial manufacturing for the future production of parts and supplies.[7-10] While a growing list of elastomers, plastics, and composites have been reported, there are relatively few examples of resins that are bio-sourced and bio-degradable.[11,12] The design of photocurable resins for vat photopolymerization requires photocrosslinkable molecules that have a low viscosity and fast rate of photocuring (on the order of seconds per layer). In general, a low viscosity (0.25 Pa·s to 10 Pa·s) is necessary to facilitate resin reflow and to minimize the capillary forces exerted onto the printed object during printing.[13-16] Naturally occurring polymers often require modification with photocurable functionalities to become printable. Most notably, methacryl groups have been introduced onto the amines of biopolymers to afford polymerizable materials like gelatin methacrylamide (Gel-MA),[17] silk fibroin methacrylate (Sil-MA),[18] and methacrylated bovine serum albumin (MA-BSA).[13, 19] While

4D printed structures that undergo chemical or physical changes in response to their environment are often inspired by nature, there are relatively few examples that use bio-sourced and biodegradable materials. This work expands the potential of protein-based plastics using a bovine serum albumin (BSA) based resin for 3D printing that affords shape-morphing bioplastic constructs (**Figure 1**). Moreover, we demonstrate that the inherent globular shape of BSA – and the release of its "stored length" is critical to the plasticity of these materials.

Structural and globular proteins are known as macromolecules that can introduce material plasticity or elasticity based on the unfolding or disassembly of the proteins.[20,21] Spider silk is a structural protein that has a specific energy to failure (160 J/g) that is greater than Kevlar (50 J/g) and is attributed to the presence of β-sheet domains.[22-24] Single molecule atomic force microscopy (AFM) experiments on titin by Gaub and co-workers showed that proteins can be unraveled reversibly or irreversibly upon the application of a tensile force.[25] Since then, the secondary and tertiary structure of proteins have been utilized to achieve biomaterials with unique combinations of extensibility, strength, and resilience. More recently, BSA was incorporated into hydrogel networks to provide an energy dissipation mechanism via protein unfolding.[26,27] However, there has not been a demonstration of a protein-based material that exhibits plasticity due to unfolding, with a corresponding shape recovery back to its original form. BSA is a globular protein comprised of a single macromolecular chain that is precisely folded to comprise 67% alpha helices and 17 disulfide bonds. Within a photopolymerized network of these globular proteins, each protein molecule can be unfolded to release its "stored length" as a mechanism of energy dissipation. Furthermore, we demonstrate that the incorporation of plasticity within a cross-linked thermoset affords a mechanism for shape recovery after the object has been plastically deformed.
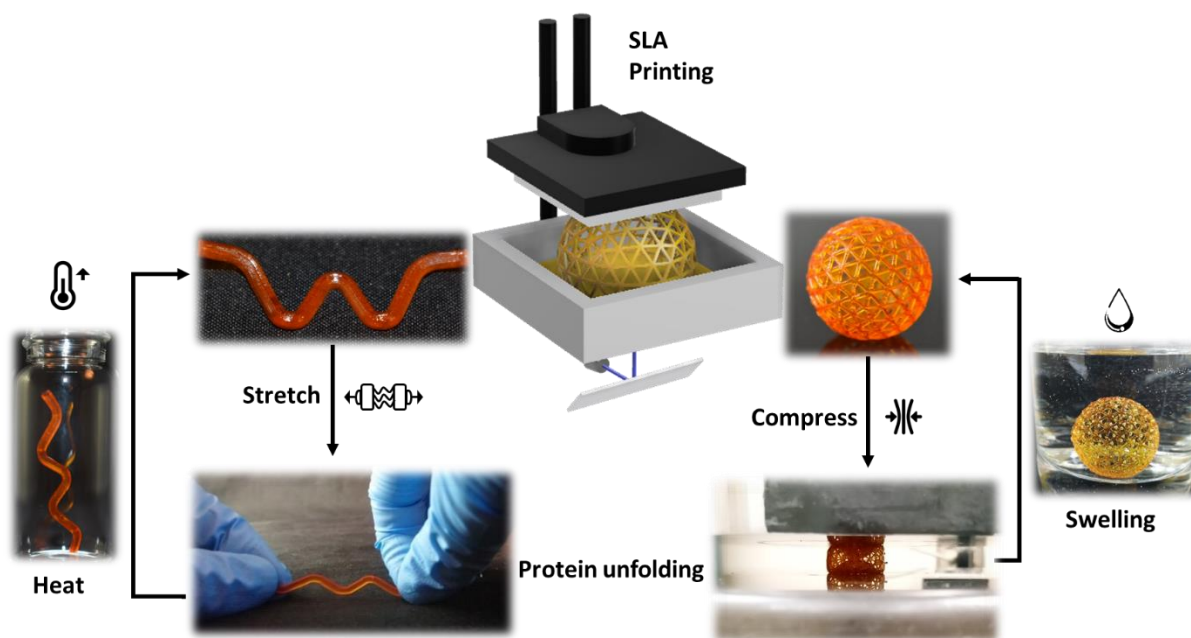
Figure 1. General scheme for SLA 3D printing and shape recovery process. Objects were 3D printed and then dried to afford a 3D bioplastic object. The printed objects were plastically deformed by compression or elongation to afford a metastable state, and recovered their original shape upon heating or swelling in an aqueous solution.

2. MATERIALS AND METHODS

General Methods. All materials were purchased from Sigma-Aldrich unless otherwise stated. Tris(2,2′-bipyridyl)-dichlororuthenium(II) hexahydrate (Ru(bpy)$_3$Cl) (99.95%), poly-(ethylene glycol) diacrylate (Mn = 700 g/mol), and sodium persulfate (SPS) were used as received. Ultrapure and ultralow fatty acid content BSA was purchased from Nova Biologics. Formlabs standard clear resin (FLGPCL04) was purchased from Formlabs. Ultraviolet-visible spectra were recorded with a Varian Cary 5000 UV-Vis-NIR spectrophotometer and a 1 cm path quartz cuvette, and data collection and analysis were carried out with Cary WinUV software. Thermal analyses were conducted on a Mettler Toledo DSC 3+ differential scanning calorimeter (DSC). All scans were carried out in hermetic aluminum pans under a nitrogen atmosphere for sample weights between

5 and 10 mg. For the purpose of studying transition temperatures, scans were performed from 50 ºC to 200 ºC with a scan rate of 10 ºC/min. Attenuated Total Reflection Fourier Transform Infrared (ATR-FTIR) spectroscopy was performed with a Perkin Elmer Frontier FTIR spectrometer with a mounted Universal ATR Sampling Accessory. Spectra were taken with a resolution of 4 cm^{-1} and were averaged over 32 scans in the 4000-400 cm^{-1} range, and data collection and analysis were carried out with PerkinElmer Spectrum software.

BSA-Based Resin Preparation Protocol. The weight percentages are based on the total composition of the resin, including the aqueous solvent. As a representative example, we describe here the preparation of 20 g of resin with 30 wt % BSA and 10 wt % poly(ethylene glycol) diacrylate (PEG-DA). First, 2 g of PEG-DA were dissolved in 11.2 mL of DI water, then 6 g of BSA was slowly added to this solution with gentle mixing until well dissolved. Next, 15 mg Ru(bpy)$_3$Cl dissolved in 400 μL of DI water and 48 mg SPS dissolved in 400 μL of DI water were sequentially dissolved into the resin formulation. The final resin formulation was covered in aluminum foil and stored at 4 °C until use. To prepare other formulations, the same procedure was followed, changing only the comonomer and DI water quantities.

Rheology. Rheology measurements were performed on a TA Instruments Discovery Hybrid Rheometer-2. Viscosity versus shear rate experiments were performed at a shear rate increasing from 1 to 100 s^{-1} using a 40 mm cone and plate geometry with a cone angle of 1.019°, a solvent trap, and a gap height of 26 μm. To conduct photorheology experiments, a 365 nm LED UV-curing accessory with disposable acrylic plates was used. The photorheological experiments were conducted using constant 1% strain and a frequency of 1 Hz, and a 20 mm parallel plate with a gap height of 1000 μm. A 60 s dwell time elapsed before the UV lamp was turned on for 5 min. Data collection and analysis were carried out with TRIOS software (TA Instruments).

3D Printing. A Formlabs Form 2 printer was used to fabricate the 3D printed constructs, but the build plate and resin tray were modified to reduce the total volume of resin required to print. The build plate was cut down to 45 mm × 45 mm, and a 48 mm × 78 mm × 28 mm border was 3D printed on a Flashforge Creator Pro, then glued to the resin tray to form a small reservoir within the standard resin tray. 3D constructs were designed with Autodesk Fusion 360 or downloaded from Thingiverse. The resin was poured into the reservoir, and the bioplastic constructs were then printed in the Form 2's Open Mode with a layer height of 100 μm. The Form 2 SLA printer uses a 405 nm violet laser (250 mW) with a laser spot size of 140 microns. The duration of the light exposure for each layer was approximately 30 s. Upon completion of the print, samples were removed from the build plate, rinsed in DI water to remove any uncured resin, and then air-dried. No post-curing process was needed. Some samples were further thermally cured by placing them in a 120 °C oven for 180 min.

Circular Dichroism. The secondary structure of BSA within the resin was determined by circular dichroism using a Jasco J-815 spectropolarimeter. The BSA-based resin was prepared at a final BSA concentration of 100 μM, while maintaining the relative concentrations of the other components (10 wt % PEG-DA + 30 wt % BSA + 0.075 wt % $Ru(bpy)_3Cl$ + 0.24 wt % SPS + 59.685 wt % DI water). A thin film of the protein-resin mixture was then formed on a 1 cm² quartz slide, by spin-coating 40 μL of the material at an angular speed of 3000 RPM for 10 min on a Laurell Technologies corporation Model WS-400B-6NPP/LITE spin-coater. The newly formed thin film was immediately UV-cured for 1.5 h, using a 405 nm lamp at maximum power placed at a distance of 2 cm. A thermal treatment was then performed on the solid film, heating the quartz slide at 120 °C for 1 h. The CD spectrum of the material was monitored after each step, using 1 nm increments and 8 second integration time over a wavelength range of 190 to 260 nm.

Mechanical Properties. Tensile tests were performed with a TA Electroforce TestBench uniaxial tension instrument at a speed of 6 mm/min until mechanical failure of the sample. The dogbones were 3D printed in the Form2 SLA printer, following ISO 527-2 (ISO 527-2/5B/6). Cylindrical compression samples (10 mm diameter × 5 mm height) were 3D printed and dried, before being tested with an Instron 5585H 250 kN electro-mechanical test frame with a 50 kN load cell using a crosshead rate of 1.3 mm/min. All the specimens were first air-dried overnight, and then vacuum-dried during at least 24 hours prior to the mechanical test.

Thermal Transitions. The steady state mechanical behavior of the samples was determined by dynamic mechanical thermal analysis (DMTA) measurements, conducted in compression mode in a Dynamic Mechanical Analyzer, Triton 2000 DMA (Triton Technology). Cylindrical samples (4.1 mm x 7.6 mm; thickness x diameter) were heated from -50 °C to 150 °C at a constant heating rate of 4 °C/min and at a frequency of 1 Hz.

3. RESULTS AND DISCUSSION

3.1. Formulation and Printability of the BSA-Based Resin for Vat Photopolymerization. We previously reported a methacrylated BSA (MABSA),[13] in which methacrylic anhydride was used to functionalize BSA, and the MABSA product was isolated after dialysis. In this work, we have simplified the resin formulation by using an aza-Michael addition reaction between the surface lysines of BSA and an acrylate of poly(ethylene glycol) diacrylate (PEG-DA) for the *in situ* functionalization of BSA with acrylates (**Figure 2a**). This simplifies the resin formulation because a separate purification step is no longer required. An aqueous resin comprised of BSA and poly(ethylene glycol) diacrylate (PEG-DA) was optimized for the Form 2 printer by using a rheometer to characterize the viscosity (<10 Pa·s) and rate of photo-curing based on the storage

modulus (G') (>3 kPa/s) during the first seconds of UV light irradiation (**Figure S1** and **Table S1**). Although BSA can undergo slow photo-induced crosslinking on its own (attributable to its tyrosine residues),[28, 29] the rate of curing was insufficient to afford mechanically stable networks during the printing process. The addition of PEG-DA (M_n = 700 g/mol) as a second reactive monomer resulted in aqueous formulations that could undergo rapid photo-initiated transformation into a 3D patterned hydrogel during the printing process. In comparison, a resin comprised of 30 w/w % of BSA without the addition of a comonomer required 140 s of irradiation before the storage modulus began to increase, whereas the addition of 3 w/w % of PEG-DA to this formulation resulted in an immediate change to the storage modulus upon irradiation (see **Figure S1a**). We hypothesized that the lysine residues on the surface of BSA react with the acrylates of PEG-DA via an *aza*-Michael addition, which was confirmed by the absence of reactive amines in a 2,4,6-trinitrobenzenesulfonate (TNBS) assay (78 % of the available lysine residues were functionalized), and the appearance of a peak near 1530 cm^{-1} corresponding to the secondary amines (N–H in-plane bending) at the IR spectrum (**Figure S2**). The BSA was functionalized *in situ* with acrylates, and as a result, these formulations underwent a significantly faster rate of photocuring while keeping the low viscosity required for the resin to reflow (**Figure 2b**). The optimal photocurable resin was composed of 30 w/w % BSA, 10 w/w % PEG-DA, 0.075 w/w % ruthenium tris(bipyridyl) chloride (Ru(bpy)$_3$Cl), and 0.24 w/w % sodium persulfate (SPS), which was determined after evaluating the viscosity and photocuring rates of different resin formulations (**Table S1**). Based on previous studies with MA-BSA,[13] we determined that the ideal viscosity ranges from 0.25 to 10 Pa·s (to allow the resin to reflow), and the rate of photocuring needed to exceed 3 kPa/s (based on the change in storage modulus during the first 30 s of irradiation) for resins with good printability. For this particular formulation, viscosity was 1.3 Pa·s, and the rate

of photocuring was 7.8 kPa/s. The as-printed 3D construct is a hydrogel that de-swells isotropically upon dehydration to afford a 3D patterned bioplastic that is ca. 75% protein in content. Objects with different 3D printed geometries were printed by changing the CAD model, and in all cases, the bioplastic retained the same geometries and shapes as the printed hydrogel but with 30 % smaller dimensions (**Figure S3**).
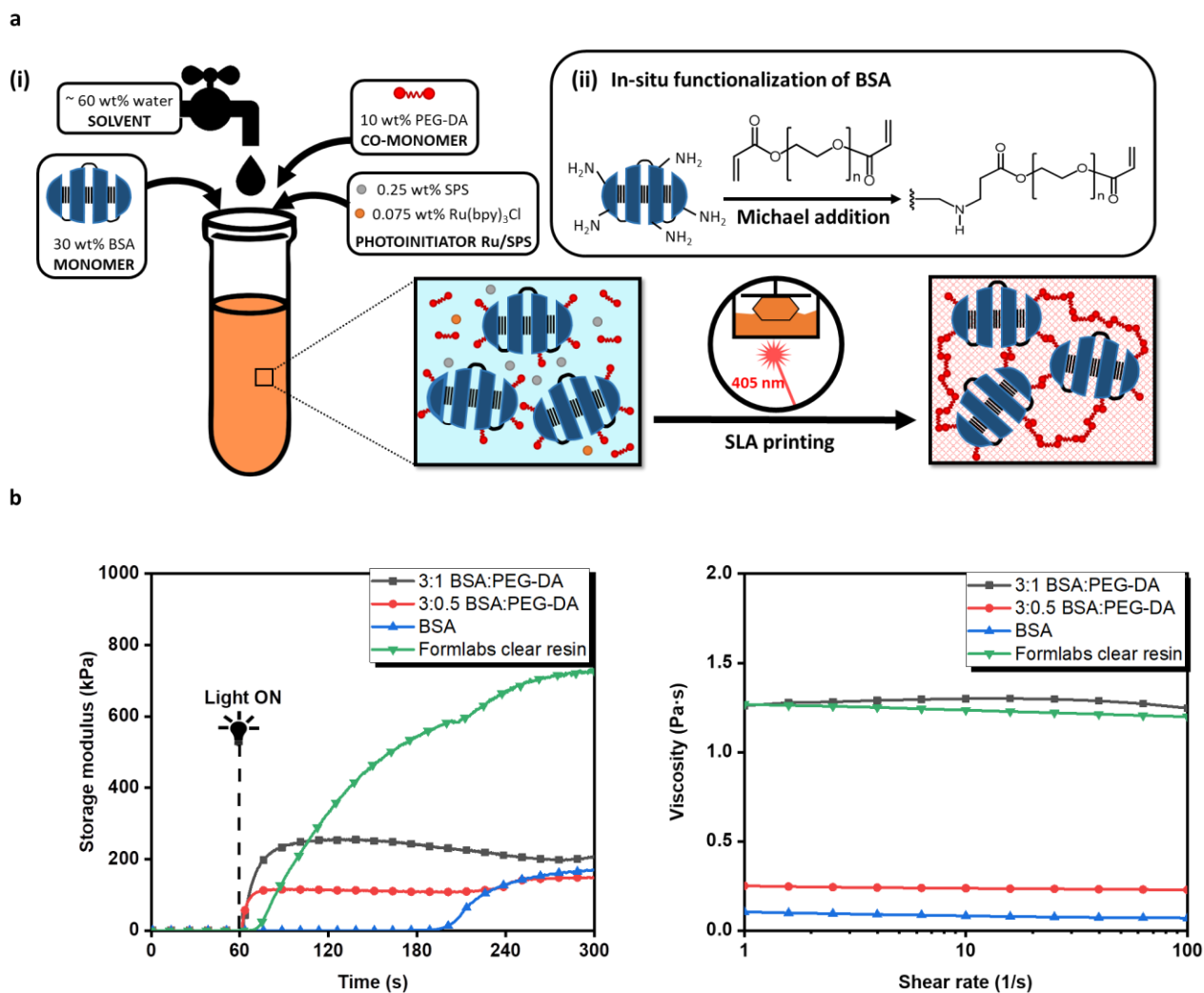
Figure 2. Resin formulation and printability. (a) Schematic showing the resin preparation: (i) Formulation of the optimized photopolymerizable resin composed of 30 wt % BSA, 10 wt % PEG-DA, 0.24 wt % SPS, 0.075 wt % Ru(bpy)$_3$Cl, and 59.685 wt % DI water, and (ii) *aza*-Michael addition reaction between the surface lysine amines of BSA and the acrylates of PEG-DA (excess) occurred *in situ* to afford a photocurable aqueous mixture. (b) The aqueous resins were characterized by rheometry to determine the (i) the rate of photocure, and (ii) viscosity for each of the resins investigated. For comparison, the rheological measurements of a commercial SLA resin (Formlabs clear resin) are also shown.

3.2. Tailoring the Macroscopic Properties of the BSA-Based 3D Printed Bioplastic Using the Unfolding Mechanisms of the Globular Proteins. As demonstrated by circular dichroism (CD) spectroscopy, the BSA proteins maintain their conformation—both, in the aqueous resin and the photocured bioplastic (**Figure 3a**). The spectrum of the photocured resin after dehydration was characteristic of BSA in its folded conformation with two negative peaks around 210 and 222 nm, as well as the positive peak around 195 nm that reflected the high alpha-helical content of the protein. BSA is known to denature in solution at temperatures above 90 °C,[30] temperature that was also confirmed in our dried bioplastics using differential scanning calorimetry (DSC) (**Figure S4**). The unfolding process of the proteins is an endothermic event that requires the input of energy, such as heat or force, to endow the proteins with internal mobility. Thermal treatment of 3D printed and dehydrated bioplastics (at 120 °C) caused the unfolding of the native BSA structure, which was reflected by the featureless CD spectrum (**Figure 3a**). This change in the secondary structure of the protein was also supported by the ATR-FTIR spectra in **Figure 3b**. The amide I region of the spectrum showed a band at 1648 cm^{-1}, which was indicative of α-helical conformations, which decreased in favor of a new resonance at 1622 cm^{-1} for the β-sheet interactions after thermal cure.[31,32] Finally, the absence of thermal transitions observed after the heat treatment of the samples in the dynamic mechanical thermal analysis (DMTA) corroborates the unfolding of the native BSA (**Figure 3d**).

The β-sheet formation during thermal cure enhanced the stiffness of the materials, as demonstrated by the increase in the elastic modulus and strength of the thermally cured bioplastic (**Figure 3c** and **Figure S5**).[33] This result was consistent with the presence of more intermolecular hydrogen bonding interactions between protein molecules. The 3D printed bioplastic samples that were thermally cured to denature the globular proteins prior to mechanical analysis exhibited

brittle fracture. The tensile strength was 46 MPa, while elongation at break was 25 %. In contrast, the samples that were not thermally cured behaved as thermoplastic materials, with a clear yielding behavior upon stretching. The elongation at break increased to 61 %, and the toughness (10.6 J/m^3) improved relative to the thermally cured and denatured samples (5.3 J/m^3).[21] Thus, the folded globular proteins introduced a molecular plasticity, wherein the proteins were unfolded under tensile strain to release their stored length. This demonstration illustrates how the secondary structure of these 3D printed protein constructs can be transformed from a thermoplastic to a thermoset using the same material composition (**Figure 3e**).
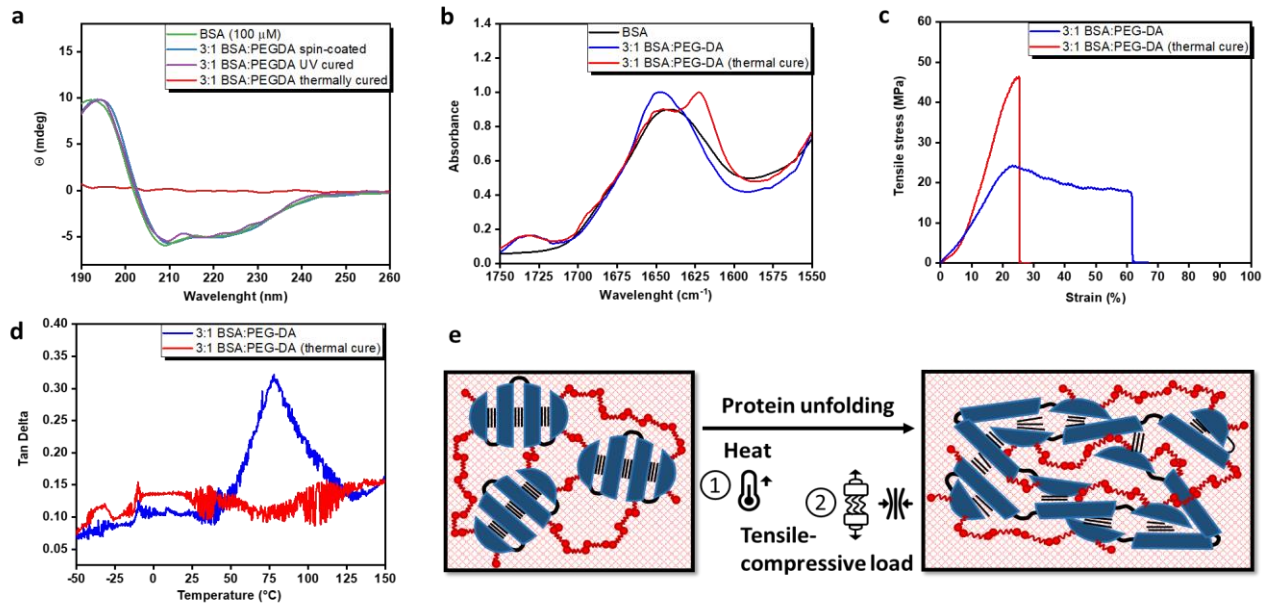
Figure 3. Thermally or mechanically induced protein unfolding in the 3D printed bioplastic constructs. (a) Solid state circular dichroism spectra showed that the BSA maintained its conformation after photocuring, but that this structure was lost after thermal cure (120 °C). (b) ATR-FTIR spectra of the amide region shows the transition of the α-helical structure of BSA into β-sheets after thermal cure. (c) Representative uniaxial tensile stress-strain curve comparing thermally cured ($\sigma_{max} = 46$ MPa) and non-thermally cured ($\sigma_{max} = 24$ MPa) samples; the ductility observed in the non-thermally cured sample is lost in the thermally cured sample as a result of the increased presence of intermolecular β-sheets that were formed. (d) DMTA spectrum showed a glass transition at 78 °C. (e) Schematic depicting the unfolding of BSA as a consequence of either thermal treatment or mechanical load (tensile or compressive).

13

3.3. Shape recovery of mechanically deformed bioplastics. Based on the plasticity observed with these cross-linked thermosets (non-thermally cured), we next investigated the shape-recovery of mechanically deformed 3D printed constructs. As shown in **Figure 4**, objects with different geometries (cylindrical puck, hollow spherical lattice, solid sphere, "W" shaped tube, and a deployable stent) were 3D printed and dehydrated to afford bioplastic constructs that were either compressed, elongated or hydrated at ambient temperature. All of the mechanically deformed constructs maintained this shape for at least 6 months at ambient conditions. Each of these shapes recovered from their nonequilibrium shape when subjected to heating (~120 °C) or rehydration in water (**Figure 4a** and **Videos S1, S2**). While the ductility of the 3D printed objects was derived from the release of the stored length in the globular proteins, the transition back to the respective equilibrium shapes was driven by the presence of the covalently cross-linked network that was produced during the photo-initiated polymerization.[21,27]

At high compressive strains, mechanical damage was observed in the bioplastic materials, but shape recovery was still achieved. However, when a compressive load of 20 % was applied, there was no visible evidence of mechanical damage, and the 3D printed object could undergo over ten cycles of compression and thermal shape recovery with small increases to the compressive modulus with each cycle (**Figure S6**). The secondary and tertiary structure of the proteins after shape recovery is not known, although it is unlikely that the proteins refold into their globular shape within these printed constructs. Nevertheless, the rapid shape recovery behavior of these bioplastics, which can occur in a matter of seconds, can be useful for the production of medical devices such as scaffolds, implants, or stents (**Figure 4b, c, d** and **Videos S3, S4**).[34] Previous studies with MA-BSA demonstrated that 3D printed BSA-based materials were not cytotoxic.[13] Further studies on the biocompatibility and biodegradation of the materials are underway.
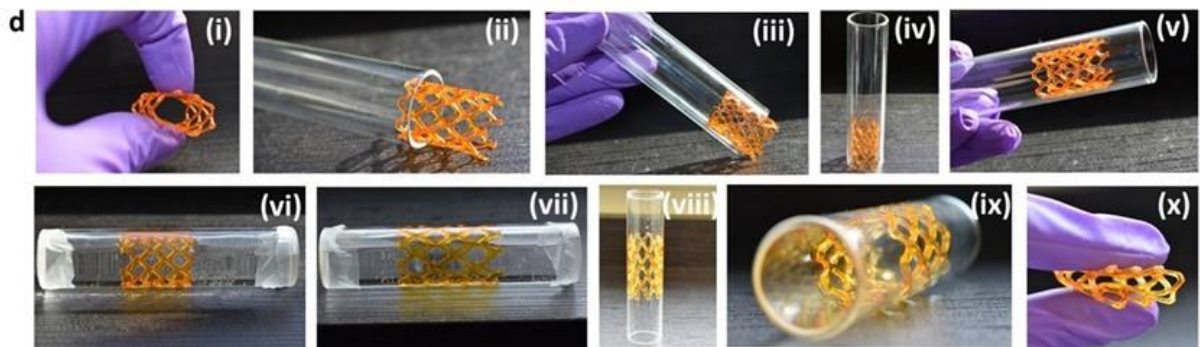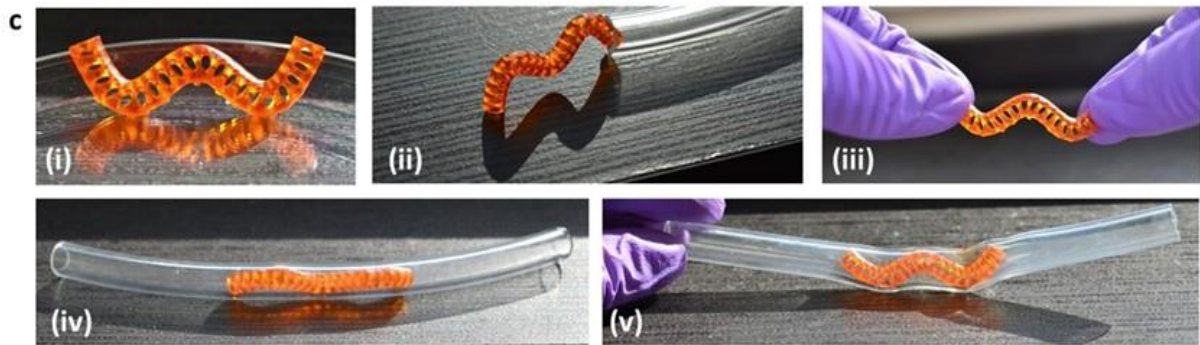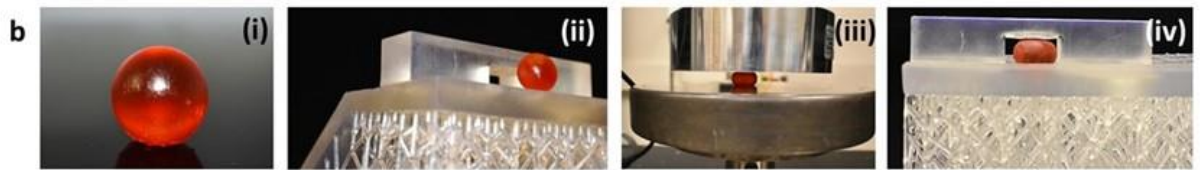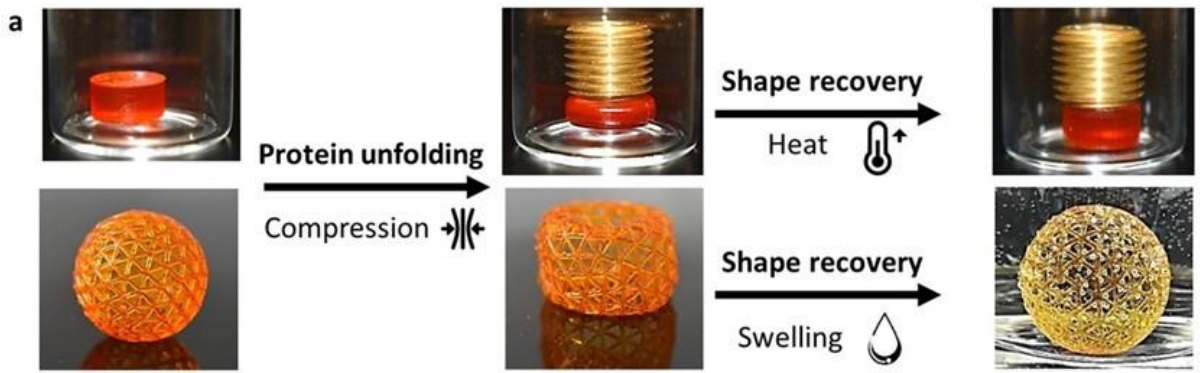
Figure 4. Shape recovery effect in 3D printed constructs. (a) Photographs showing the shape recovery process of the compressed samples using two different stimuli: heat and hydration. (b) Photographs of a solid sphere which was compressed to pass through a narrow opening: (i) a 3D printed and dehydrated sphere with a diameter of 14 mm was (ii) too large to pass through an opening (20 mm x 10 mm), (iii) the ball was compressed until it had a height of 9 mm (65 % of the original height), and (iv) slid through the gap. The spherical shape was recovered using a heat gun (Video S3). (c) Sequence of photographs showing the elongation of a printed bioplastic construct: (i) printed "W" hollow shape with an initial length of 40 mm and a height of 12 mm, (ii) could not fit through the opening of a plastic tube with diameter 6 mm; (iii) manually stretching the printed "W" until it had a length of 45 mm and a height of 5 mm, (iv) the stretched form fit within the tube, and (v) this stretched form was recovered using a heat gun bending the plastic tube during the recovery process. (d) Photographs of a 3D printed gastrointestinal stent swelled into a glass tube: (i) the printed stent was flexible in its dried state owing to the design, (ii) the external diameter of the stent was 15 mm whereas the diameter of the tube was 20 mm, therefore (iii), (iv), (v), the stent could slide freely within the glass tube. Then (vi), the tube was filled with water and closed with parafilm at the ends, and (vii) after 15 min, the stent was perfectly adapted to the interior of the glass tube due to the swelling, increasing its length from 24 mm to 32 mm (30 % bigger dimensions after swelling). When the water was emptied (viii) the stent was firmly fixed inside the tube, (ix) the stent was fitted into the tube, but (x) being the stent softer after hydration compared to the dried form, it could be removed easily from the glass tube.

4. CONCLUSIONS

In conclusion, we formulated a simple aqueous-based resin for laser-scanning SLA printing based on BSA and PEG-DA as a photocurable resin. BSA is a globular protein with excellent aqueous solubility and low viscosity at concentrations up to 30 wt%. The *in situ* modification of BSA with PEG-DA via an aza-Michael addition provides a simple means by which this protein can be modified with acrylate functionalities. Furthermore, we demonstrated that the native conformation of these globular proteins is largely retained in the 3D printed constructs, and that each protein molecule possesses a "stored length" that could be revealed during mechanical deformation (extension or compression) of the 3D bioplastic objects. Given the large molecular weight of BSA (66 kDa), the potential for unfolding individual protein chains can be significant, as exhibited by the plasticity observed in these thermoset materials. While the plastically deformed objects retained their shape for an indefinite period of time, heat or submersion in water allowed it to return to its original 3D printed shape. We expect this strategy – wherein globular proteins are utilized to afford 3D printed bioplastics with mechanical properties that utilize the stored length of these macromolecules – is broadly applicable to other forms of vat photopolymerization to create constructs that can create a closed loop life cycle with bioplastics.

ASSOCIATED CONTENT

Supporting Information

The following files are available free of charge.

Printability of different resin formulations; photo-curing rate and viscosity of different resin formulations; primary amine reaction with the acrylate groups: TNBS Assay & ATR-FTIR;

isotropic de-swelling of the printed hydrogels; DSC thermograms representing the thermal denaturation of the BSA; compression tests comparing heated and non-heated samples; mechanical properties after a number of compression & thermo-recovery cycles; and description of the supporting video material (PDF).

Shape recovery of a compressed cylinder with heat (MP4).

Shape recovery of a compressed spherical lattice with hydration (MP4).

Changing the shape of a solid sphere to pass through a rectangular cavity (MP4).

Shape recovery of a stretched W Shape with heat (MP4).

AUTHOR INFORMATION

Corresponding Author

*Alshakim Nelson - Department of Chemistry, University of Washington, Seattle, WA, USA

E-mail: alshakim@uw.edu

Author Contributions

The manuscript was written through contributions of all authors. All authors have given approval to the final version of the manuscript.

Notes

The authors declare no competing financial interests.

REFERENCES

1. Mekonnen, T.; Mussone, P.; Bressler, D., Valorization of Rendering Industry Wastes and Co-products for Industrial Chemicals, Materials and Energy: Review. *Crit. Rev. Biotechnol.* **2016,** *36* (1), 120-131.

2. Johnson, J. A.; Lu, Y. Y.; Van Deventer, J. A.; Tirrell, D. A., Residue-Specific Incorporation of Non-canonical Amino Acids into Proteins: Recent Developments and Applications. *Curr. Opin. Chem. Biol.* **2010,** *14* (6), 774-780.

3. Chan, W. Y.; Bochenski, T.; Schmidt, J. E.; Olsen, B. D., Peptide Domains as Reinforcement in Protein-Based Elastomers. *ACS Sustainable Chem. Eng.* **2017,** *5* (10), 8568-8578.

4. Verbeek, C. J. R.; van den Berg, L. E., Extrusion Processing and Properties of Protein-Based Thermoplastics. *Macromol. Mater. Eng.* **2010,** *295* (1), 10-21.

5.   Sánchez-deAlcázar, D.; Velasco-Lozano, S.; Zeballos, N.; López-Gallego, F.; Cortajarena, A. L., Biocatalytic Protein-Based Materials for Integration into Energy Devices. *ChemBioChem* **2019,** *20* (15), 1977-1985.

6.   Bier, J. M.; Verbeek, C. J. R.; Lay, M. C., Thermal Transitions and Structural Relaxations in Protein-Based Thermoplastics. *Macromol. Mater. Eng.* **2014,** *299* (5), 524-539.

7.   Gonzalez-Henriquez, C. M.; Sarabia-Vallejos, M. A.; Rodriguez-Hernandez, J., Polymers for Additive Manufacturing and 4D-Printing: Materials, Methodologies, and Biomedical Applications. *Prog. Polym. Sci.* **2019,** *94*, 57-116.

8.   Kuang, X.; Roach, D. J.; Wu, J. T.; Hamel, C. M.; Ding, Z.; Wang, T. J.; Dunn, M. L.; Qi, H. J., Advances in 4D Printing: Materials and Applications. *Adv. Funct. Mater.* **2019,** *29* (2), 1805290.

9.   Quan, H.; Zhang, T.; Xu, H.; Luo, S.; Nie, J.; Zhu, X., Photo-Curing 3D Printing Technique and Its Challenges. *Bioact. Mater.* **2020,** *5* (1), 110-115.

10.   Ligon, S. C.; Liska, R.; Stampfl, J.; Gurr, M.; Mulhaupt, R., Polymers for 3D Printing and Customized Additive Manufacturing. *Chem. Rev.* **2017,** *117* (15), 10212-10290.

11.   Narupai, B.; Nelson, A., 100th Anniversary of Macromolecular Science Viewpoint: Macromolecular Materials for Additive Manufacturing. *ACS Macro Lett.* **2020,** *9* (5), 627-638.

12.   Sanchez-Rexach, E.; Johnston, T. G.; Jehanno, C.; Sardon, H.; Nelson, A., Sustainable Materials and Chemical Processes for Additive Manufacturing. *Chem. Mater.* **2020,** *32* (17), 7105-7119.

13.   Smith, P. T.; Narupai, B.; Tsui, J. H.; Millik, S. C.; Shafranek, R. T.; Kim, D.-H.; Nelson, A., Additive Manufacturing of Bovine Serum Albumin-Based Hydrogels and Bioplastics. *Biomacromolecules* **2020,** *21* (2), 484-492.

14.   Mondschein, R. J.; Kanitkar, A.; Williams, C. B.; Verbridge, S. S.; Long, T. E., Polymer Structure-Property Requirements for Stereolithographic 3D Printing of Soft Tissue Engineering Scaffolds. *Biomaterials* **2017,** *140*, 170-188.

15.   Schuller-Ravoo, S.; Teixeira, S. M.; Feijen, J.; Grijpma, D. W.; Poot, A. A., Flexible and Elastic Scaffolds for Cartilage Tissue Engineering Prepared by Stereolithography Using Poly(trimethylene carbonate)-Based Resins. *Macromol. Biosci.* **2013,** *13* (12), 1711-1719.

16.   Luo, Y.; Le Fer, G.; Dean, D.; Becker, M. L., 3D Printing of Poly(propylene fumarate) Oligomers: Evaluation of Resin Viscosity, Printing Characteristics and Mechanical Properties. *Biomacromolecules* **2019,** *20* (4), 1699-1708.

17.   Shirahama, H.; Lee, B. H.; Tan, L. P.; Cho, N. J., Precise Tuning of Facile One-Pot Gelatin Methacryloyl (GelMA) Synthesis. *Sci. Rep.* **2016,** *6*, 31036.

18.   Kim, S. H.; Yeon, Y. K.; Lee, J. M.; Chao, J. R.; Lee, Y. J.; Seo, Y. B.; Sultan, M. T.; Lee, O. J.; Lee, J. S.; Yoon, S.-i.; Hong, I.-S.; Khang, G.; Lee, S. J.; Yoo, J. J.; Park, C. H., Precisely Printable and Biocompatible Silk Fibroin Bioink for Digital Light Processing 3D Printing. *Nat. Commun.* **2018,** *9*, 1620.

19.   Ferracci, G.; Zhu, M.; Ibrahim, M. S.; Ma, G.; Fan, T. F.; Lee, B. H.; Cho, N.-J., Photocurable Albumin Methacryloyl Hydrogels as a Versatile Platform for Tissue Engineering. *ACS Appl. Bio Mater.* **2020,** *3* (2), 920-934.

20.   Fang, J.; Mehlich, A.; Koga, N.; Huang, J.; Koga, R.; Gao, X.; Hu, C.; Jin, C.; Rief, M.; Kast, J.; Baker, D.; Li, H., Forced Protein Unfolding Leads to Highly Elastic and Tough Protein Hydrogels. *Nat. Commun.* **2013,** *4*, 2974.

21.   Cera, L.; Gonzalez, G. M.; Liu, Q. H.; Choi, S.; Chantre, C. O.; Lee, J.; Gabardi, R.; Choi, M. C.; Shin, K.; Parker, K. K., A Bioinspired and Hierarchically Structured Shape-Memory Material. *Nat. Mater.* **2021**, *20*, 242–249.

22.   Cheng, M.; Chen, W. N.; Weerasooriya, T., Mechanical Properties of Kevlar (R) KM2 Single Fiber. *J. Eng. Mater. Technol.* **2005,** *127* (2), 197-203.

23.   Papkov, D.; Zou, Y.; Andalib, M. N.; Goponenko, A.; Cheng, S. Z. D.; Dzenis, Y. A., Simultaneously Strong and Tough Ultrafine Continuous Nanofibers. *ACS Nano* **2013,** *7* (4), 3324-3331.

24.   Chan, N. J.; Gu, D.; Tan, S.; Fu, Q.; Pattison, T. G.; O'Connor, A. J.; Qiao, G. G., Spider-Silk Inspired Polymeric Networks by Harnessing the Mechanical Potential of Beta-Sheets Through Network Guided Assembly. *Nat. Commun.* **2020,** *11* (1), 1630.

25.   Rief, M.; Gautel, M.; Oesterhelt, F.; Fernandez, J. M.; Gaub, H. E., Reversible Unfolding of Individual Titin Immunoglobulin Domains by AFM. *Science* **1997,** *276* (5315), 1109-1112.

26.   Zhao, L.; Zhang, X.; Luo, Q.; Hou, C.; Xu, J.; Liu, J., Engineering Nonmechanical Protein-Based Hydrogels with Highly Mechanical Properties: Comparison with Natural Muscles. *Biomacromolecules* **2020**, *21*, 4212-4219.

27.   Khoury, L. R.; Popa, I., Chemical Unfolding of Protein Domains Induces Shape Change in Programmed Protein Hydrogels. *Nat. Commun.* **2019,** *10*, 5439.

28.   da Silva, M. A.; Lenton, S.; Hughes, M.; Brockwell, D. J.; Dougan, L., Assessing the Potential of Folded Globular Polyproteins As Hydrogel Building Blocks. *Biomacromolecules* **2017,** *18* (2), 636-646.

29.   Khoury, L. R.; Slawinski, M.; Collison, D. R.; Popa, I., Cation-Induced Shape Programming and Morphing in Protein-Based Hydrogels. *Sci. Adv.* **2020,** *6* (18), eaba6112.

30.   Rombouts, I.; Lagrain, B.; Scherf, K. A.; Lambrecht, M. A.; Koehler, P.; Delcour, J. A., Formation and Reshuffling of Disulfide Bonds in Bovine Serum Albumin Demonstrated Using Tandem Mass Spectrometry with Collision-Induced and Electron-Transfer Dissociation. *Sci. Rep.* **2015,** *5*, 12210.

31.   Litvinov, Rustem I.; Faizullin, Dzhigangir A.; Zuev, Yuriy F.; Weisel, John W., The α-Helix to β-Sheet Transition in Stretched and Compressed Hydrated Fibrin Clots. *Biophys. J.* **2012,** *103* (5), 1020-1027.

32.   Cebe, P.; Hu, X.; Kaplan, D. L.; Zhuravlev, E.; Wurm, A.; Arbeiter, D.; Schick, C., Beating the Heat - Fast Scanning Melts Silk Beta Sheet Crystals. *Sci. Rep.* **2013,** *3* (1), 1130.

33.   Ma, L.; Yang, Y. H.; Yao, J. R.; Shao, Z. Z.; Chen, X., Robust Soy Protein Films Obtained by Slight Chemical Modification of Polypeptide Chains. *Polym. Chem.-UK* **2013,** *4* (21), 5425-5431.

34.   Gomes, C. M.; Liu, C.; Paten, J. A.; Felton, S. M.; Deravi, L. F., Protein-Based Hydrogels that Actuate Self-Folding Systems. *Adv. Funct. Mate.r* **2019,** *29* (4), 1805777.

For Table of Contents Only